Supporting Information

Electronic modulation of Fe–N_4 sites by second-shell sulfur for enhanced oxygen reduction electrocatalysis

Jiayun Wu[a], Xiangxiong Chen*[a], Jing Hu*[b], Dong Qian[a] and Jinlong Liu*[a]

[a] College of Chemistry and Chemical Engineering, Central South University, Changsha, 410083, China

[b] Department of Materials Science and Engineering, Southern University of Science and Technology, Shenzhen 518055, China

* Corresponding author: 30663804@qq.com; guizhouhujing_88@163.com; liujinlong@csu.edu.cn

Supporting information for the experimental section

Reagents and chemicals

All reagents were commercially available and used as received without further purification. γ-Cyclodextrin (γ-CD) and hydroxylamine hydrochloride ($NH_2OH·HCl$) were supplied by Aladdin Reagent Co., Ltd. (Shanghai, China). Iron(III) nitrate nonahydrate ($Fe(NO_3)_3·9H_2O$) and L-cysteine were purchased from Sinopharm Chemical Reagent Co., Ltd.

Synthesis of Fe−NS−C

The Fe–NS–C catalyst was prepared via a one-step pyrolysis strategy. Typically, 1.44 g of γ-CD was dispersed in 15 mL of deionized water, followed by the addition of 4 mL of an aqueous $Fe(NO_3)_3·9H_2O$ solution (10 mg mL^{-1}) under ultrasonication to form a homogeneous solution (Solution A). In parallel, 2.78 g of $NH_2OH·HCl$ and 145.4 mg of L-cysteine were dissolved in another 15 mL of deionized water under ultrasonication (Solution B). Solution B was then slowly added to Solution A, and the mixture was stirred at room temperature for 12 h. The resulting precursor was freeze-dried for 48 h, ground into a fine powder, and subsequently calcined in a tubular furnace under an Ar atmosphere. The temperature was ramped to 900 °C at a rate of 3 °C min^{-1} and maintained for 3 h. The final product was denoted as Fe–NS–C.

Synthesis of Fe−N−C and NS−C

For comparison, the Fe–N–C (without S) and NS–C (without Fe) control samples were synthesized following an identical procedure, except that L-cysteine or the iron source was omitted from the precursor solutions, respectively.

Materials characterization

The crystal structures of the samples were analyzed by X-ray diffraction (XRD, Rigaku MiniFlex 600) using Cu Kα radiation (λ = 1.5406 Å) at a scan rate of 5° min^{-1} over a 2θ range of 10–80°. Raman spectra were recorded on a Renishaw InVia Reflex Raman microscope with an excitation laser wavelength of 532 nm. Morphological and

microstructural analyses were conducted using field-emission scanning electron microscopy (FE-SEM, JSM-7610FPlus) and transmission electron microscopy (TEM, Tecnai G2 F20). High-resolution TEM (HRTEM), selected-area electron diffraction (SAED), and elemental mapping were also performed on the same TEM instrument. The surface elemental composition and chemical states were investigated by X-ray photoelectron spectroscopy (XPS, PHI VersaProbe 4). Nitrogen adsorption–desorption isotherms were collected on a Micromeritics ASAP 2460 apparatus at 77 K, and the specific surface area was calculated using the Brunauer–Emmett–Teller (BET) method. The contents of metal elements (e.g., Fe and Zn) were identified by inductively coupled plasma optical emission spectrometry (ICP-OES, PerkinElmer Avio500, Singapore).

Electrochemical measurements

All electrochemical tests were performed on a CHI 760E workstation (Chenhua Instrument, Shanghai) at room temperature. The oxygen reduction reaction (ORR) performance was evaluated in a standard three-electrode cell using 0.1 M KOH as the electrolyte, which was purged with high-purity Ar prior to measurements.

The working electrode was prepared by dispersing 5 mg of catalyst in a mixed solution containing 50 μL of 5 wt% Nafion solution, 500 μL of deionized water, and 450 μL of ethanol, followed by ultrasonication for at least 1 h to form a homogeneous ink. Subsequently, 10 μL of the ink was carefully dropped onto a pre-polished glassy carbon electrode (geometric area: 0.204 cm^2) and dried at room temperature. A Pt wire and an Ag/AgCl (saturated KCl) electrode served as the counter and reference electrodes, respectively.

Before ORR measurements, the catalysts were activated via cyclic voltammetry (CV) at a scan rate of 50 mV s^{-1} until stable curves were obtained. Linear sweep voltammetry (LSV) was then recorded at 5 mV s^{-1}. Tafel slopes were derived from the LSV curves by plotting the overpotential against the logarithm of current density (log |j|). All potentials were calibrated to the reversible hydrogen electrode (RHE) scale using the following equation:

$$E\ (\text{vs. RHE}) = E\ (\text{vs. Ag/AgCl}) + 0.197 + 0.0592 \times \text{pH}$$

Electrochemical impedance spectroscopy (EIS) was conducted at 1.064 V (vs. RHE) over a frequency range of 100 kHz to 0.1 Hz with an AC amplitude of 5 mV.

Zinc-air battery tests

Liquid zinc–air batteries (ZABs) were assembled using the as-prepared catalyst as the air cathode. The catalyst ink (described in the Electrochemical Measurements section) was uniformly loaded onto a hydrophobic carbon cloth substrate. A catalyst loading of 1 mg cm^{-2} was achieved by sequentially drop-casting 250 μL of the ink in five equal portions (50 μL each), with thorough drying at ambient temperature after each step. A polished zinc plate was used as the anode. The electrolyte consisted of 6.0 M KOH and 0.2 M $Zn(Ac)_2 \cdot 2H_2O$ in deionized water.

The open-circuit voltage (OCV) was recorded using a CHI 760E electrochemical workstation. Galvanostatic discharge, power density curves, and long-term cycling stability were evaluated on a Land CT2001A battery testing system.

Computational methods

Density functional theory (DFT) calculations were performed using the Vienna Ab initio Simulation Package (VASP) with the projector augmented wave (PAW) method.[1–3] The generalized gradient approximation (GGA) with the Perdew–Burke–Ernzerhof (PBE) functional was employed for exchange–correlation interactions.[4] A 7×4 graphene supercell doped with N and S was constructed to model the Fe single-atom catalyst (Fe-SAC) support, with a 20 Å vacuum layer along the c-axis to prevent periodic image interactions. Spin-polarized calculations were conducted to account for the magnetic properties of the Fe center. Long-range van der Waals interactions were described using the DFT-D3 method with zero-damping,[5] and the Hubbard correction (DFT+U) was applied via the Dudarev scheme[6] with an effective U value of 3.0 eV for Fe 3d orbitals to address self-interaction errors. The plane-wave cutoff energy was set to 500 eV, and the Brillouin zone was sampled using a Γ-centered 2×2×1 k-point mesh. Geometry optimizations were performed using the conjugate gradient algorithm until the maximum force on each atom was less than 0.02 eV $Å^{-1}$ and the total energy change

was below 10^{-5} eV.

Fig. S1−S6

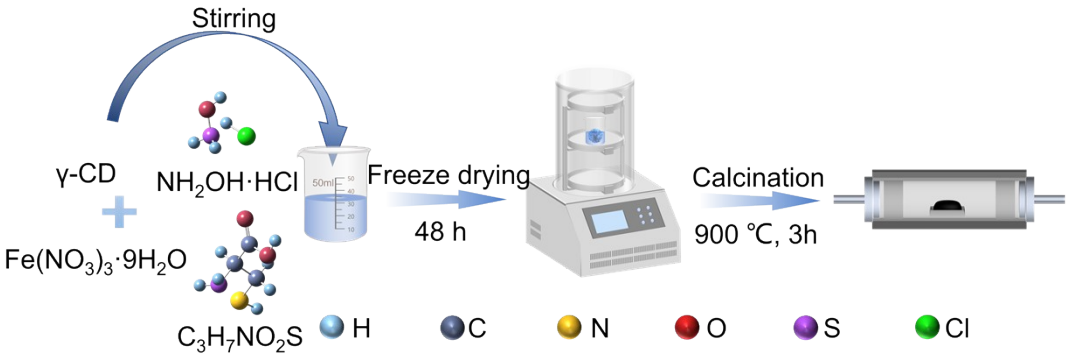

Fig. S1 Schematic illustration of the synthesis of Fe−NS−C.

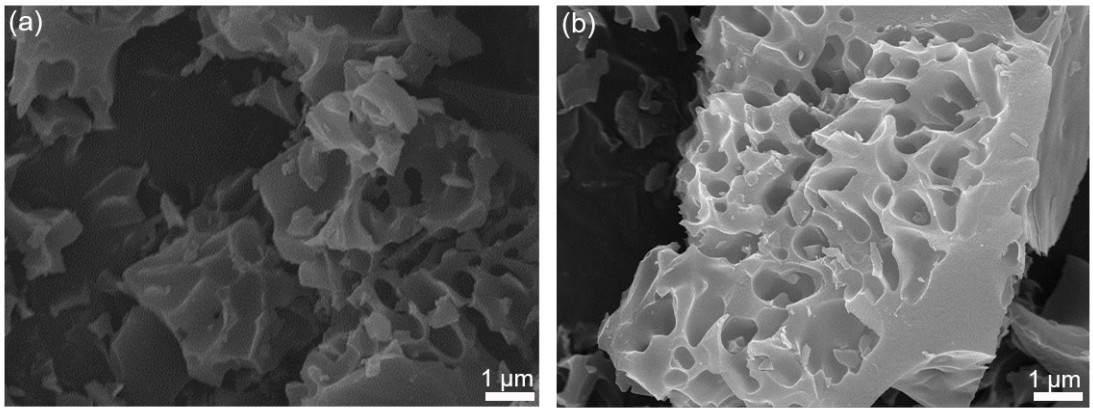

Fig. S2 Representative SEM images of (a) NS−C and (b) Fe−N−C.

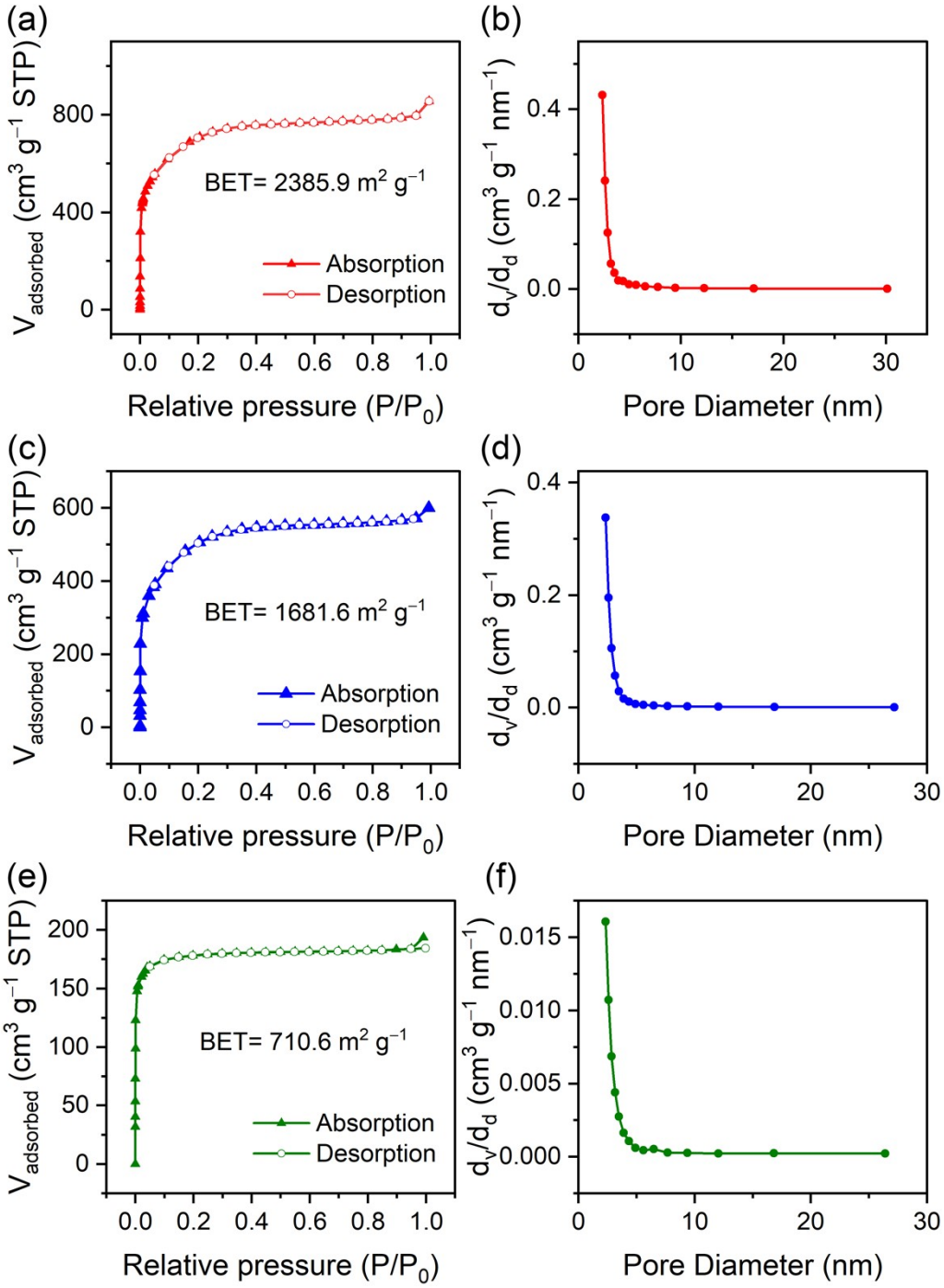

Fig. S3 N_2 adsorption-desorption isotherms (left) and corresponding pore size distributions (right) for (a,b) Fe−NS−C, (c,d) Fe−N−C, and (e,f) NS−C.

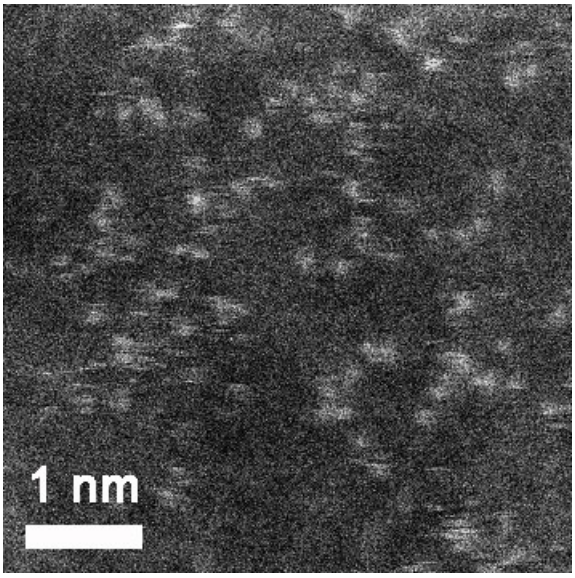

Fig. S4 Representative atomic-resolution HAADF-STEM image of Fe−NS−C. The uniformly distributed bright dots correspond to isolated Fe atoms, verifying the single-atomic nature of the catalyst.

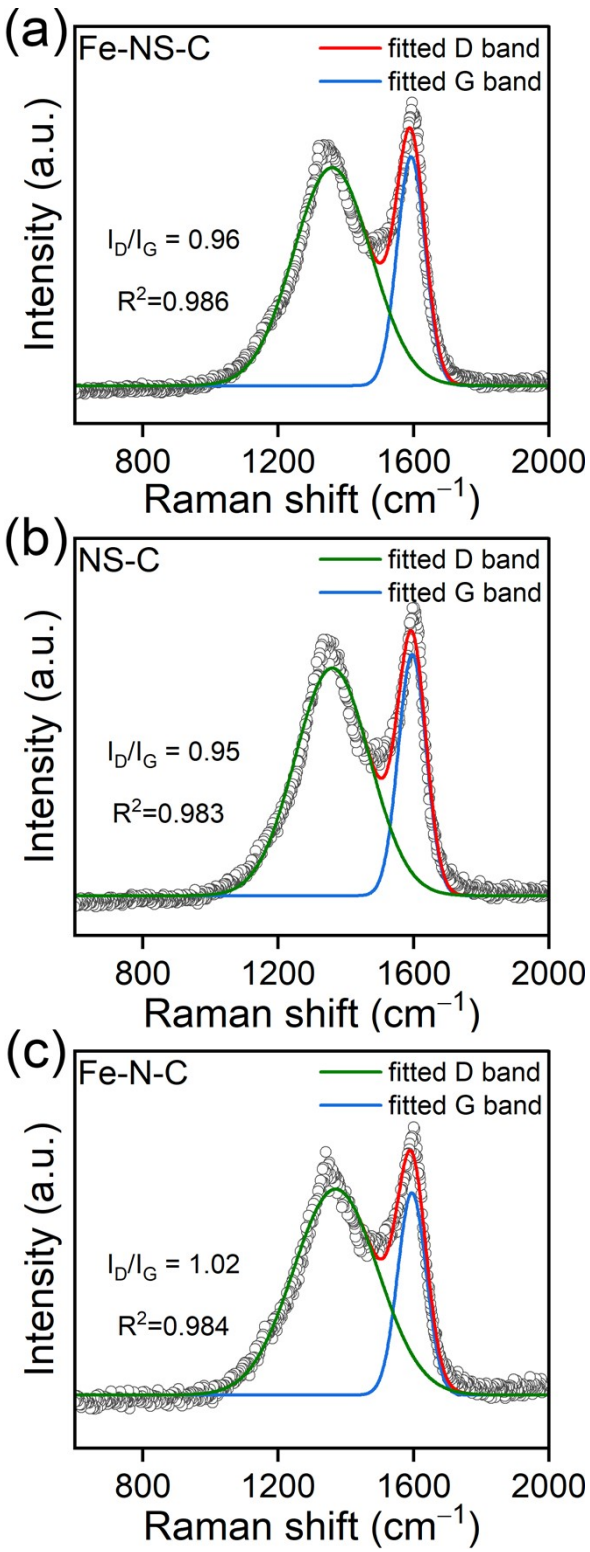

Fig. S5 Deconvoluted Raman spectra of (a) Fe−NS−C, (b) NS−C, and (c) Fe−N−C. The fitted intensity ratio (I_D/I_G) is utilized to quantify the structural defect density.

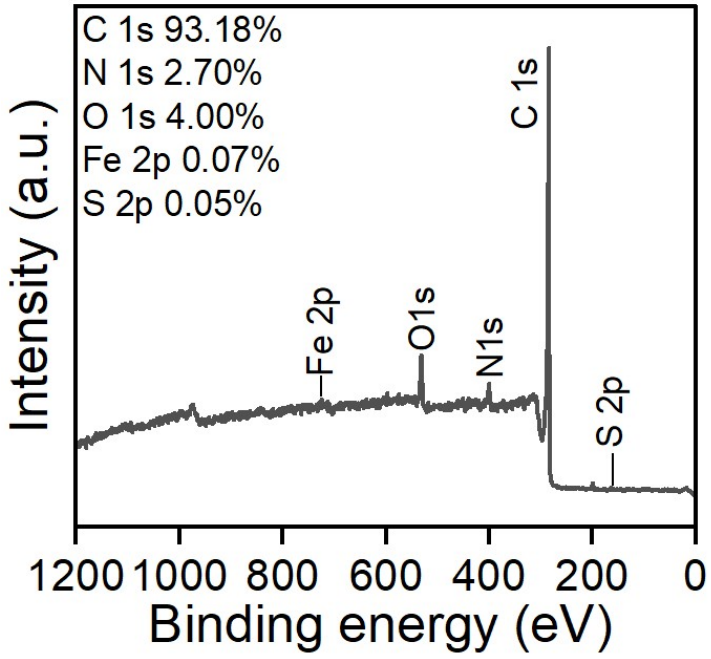

Fig. S6 XPS survey spectrum of Fe–NS–C.

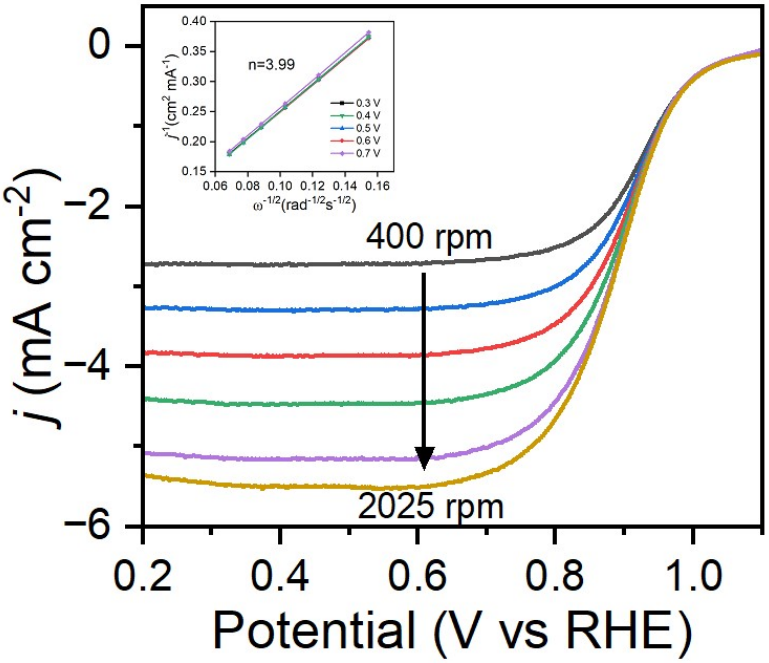

Fig. S7 LSV curves of Fe–NS–C recorded at various rotation rates ranging from 400 to 2500 rpm in 0.1 M KOH, together with the corresponding Koutecky–Levich (K–L) plots and the derived electron transfer number.

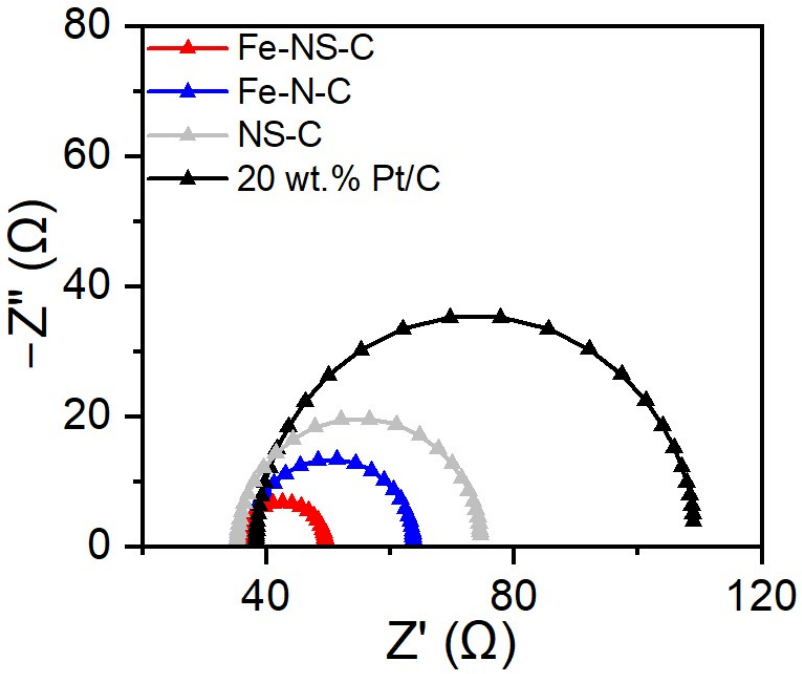

Fig. S8 Nyquist plots of Fe−NS−C, Fe−N−C, NS−C and 20 wt.% Pt/C in 0.1 M KOH.

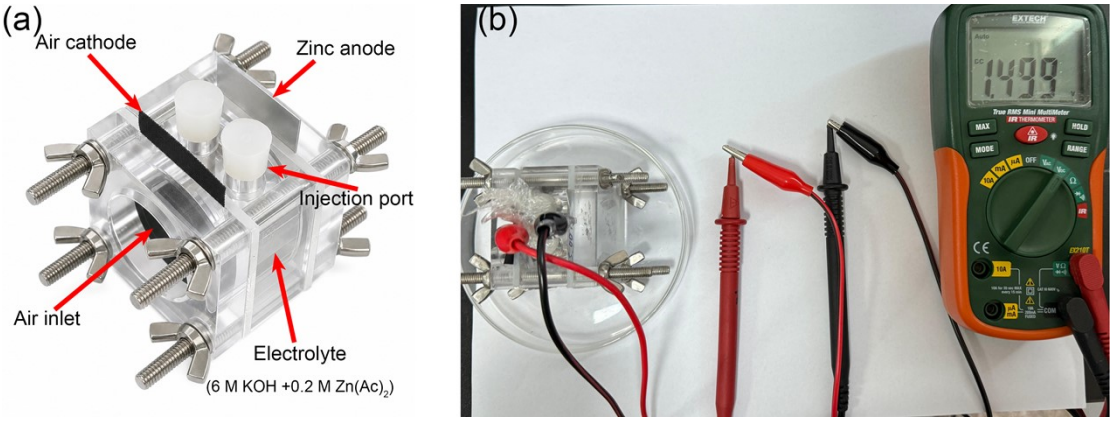

Fig. S9 (a) Photograph of a custom-fabricated liquid-type zinc–air battery setup. (b) Photograph of the open-circuit voltage of Fe-NS-C based ZAB.

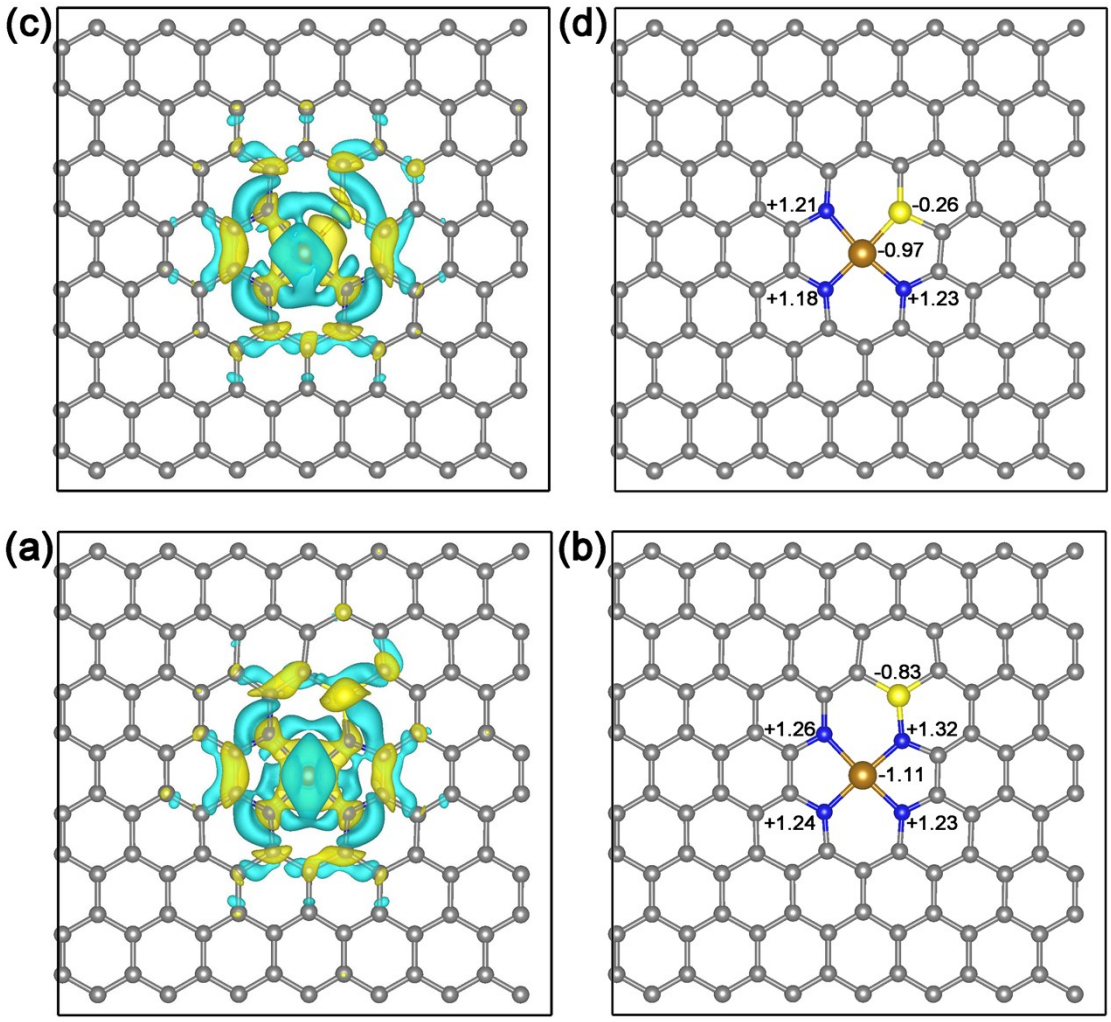

Fig. S10 Charge density difference and Bader charge analyses. (a) Isosurface plot for Fe–N_3S and (b) corresponding charge distribution. (c) Isosurface plot for Fe–N_4–S and (d) corresponding charge distribution. The yellow and cyan regions represent electron accumulation and depletion, respectively.

Table S1 Comparison of ORR catalytic activity between Fe−NS−C and other reported Fe-based electrocatalysts in 0.1 M KOH

Sample Name	$E_{1/2}$	Reference
Fe−NS−C	0.894	This work
Fe−N−C	0.878	This work
NS−C	0.860	This work
20 wt.% Pt/C	0.854	This work
Fe/NSC-800	0.83	7
Fe@NSC	0.87	8
FeCo-SN-C	0.863	9
FeS/FeSA@SNC	0.90	10
FeCo-SNC	0.856	11
Fe/SLNC	0.89	12

References

1 G. Kresse and J. Furthmüller, ***Phys. Rev. B***, 1996, **54**, 11169–11186.

2 G. Kresse and D. Joubert, ***Phys. Rev. B***, 1999, **59**, 1758–1775.

3 P. E. Blöchl, ***Phys. Rev. B***, 1994, **50**, 17953–17979.

4 J. P. Perdew, K. Burke and M. Ernzerhof, ***Phys. Rev. Lett.***, 1996, **77**, 3865–3868.

5 S. Grimme, J. Antony, S. Ehrlich and H. Krieg, ***J. Chem. Phys.***, 2010, **132**, 154104.

6 S. L. Dudarev, G. A. Botton, S. Y. Savrasov, C. J. Humphreys and A. P. Sutton, ***Phys. Rev. B***, 1998, **57**, 1505–1509.

7 H. Liu, J. Li, X. Yang, Z. Yang, W. Peng, J. Zhang, J. Li and J. Liu, ***Electrochim. Acta***, 2023, **467**, 143061.

8 D. Liu, K. Srinivas, F. Ma, H. Yu, Z. Zhang, M. Wang, Y. Wu and Y. Chen, ***J. Alloys Compd.***, 2023, **937**, 168496.

9 Z. Yang, X. Wu, G. Qin and X. Meng, ***Int. J. Hydrogen Energy***, 2025, **118**, 417–425.

10 C. Yu, Z. Yan, Y. Lin, K. Zhang, Y. Yang, G. Li, Y. Yuping, Q. Zhang and Z. Zhengyu, ***J. Colloid Interface Sci.***, 2023, **650**, 924–933.

11 Q. Huang, R. Ren, J. Li, M. Waqas, P. Chen, X. Liu, D. Huang, Z. Yang, X. Peng, D.-H. Chen, Y. Fan and W. Chen, ***Catal. Sci. Technol.***, 2024, **14**, 667–672.

12 L. Zhou, J. Yu, D. Wei, C. Shi, H. Jin, H. Li, E. Zhu and M. Xu, ***Carbon Neutral Syst.***, 2025, **1**, 18.